



## **JGR** Space Physics

#### RESEARCH ARTICLE

10.1029/2024JA032811

#### **Special Collection:**

Recent Advances on Modelling and Observations in Space and Earth Sciences

#### **Key Points:**

- Pre-midnight and dawn spikes in dB/dt occur independently; pre-midnight spikes are associated with substorm onsets
- Dawn spikes are associated with sunward-propagating, azimuthallyspaced auroral features embedded in the westward electrojet
- Fluctuations in AL associated with the dawn sector activity is often misidentified as recurrent substorm intensifications

#### Correspondence to:

S. E. Milan, steve.milan@le.ac.uk

#### Citation:

Milan, S. E., Bower, G. E., Fleetham, A. L., Imber, S. M., Schillings, A., Opgenoorth, H., et al. (2024). Occurrence and causes of large dB/dt events and AL bays in the pre-midnight and dawn sectors. Journal of Geophysical Research: Space Physics, 129, e2024JA032811. https://doi.org/10.1029/2024JA032811

Received 24 APR 2024 Accepted 20 SEP 2024

©2024. The Author(s). This is an open access article under the terms of the Creative Commons Attribution License, which permits use, distribution and reproduction in any medium, provided the original work is properly cited.

# Occurrence and Causes of Large *dB/dt* Events and AL Bays in the Pre-Midnight and Dawn Sectors

S. E. Milan<sup>1</sup>, G. E. Bower<sup>1</sup>, A. L. Fleetham<sup>1</sup>, S. M. Imber<sup>1</sup>, A. Schillings<sup>1,2</sup>, H. Opgenoorth<sup>1,2</sup>, J. Gjerloev<sup>3</sup>, L. J. Paxton<sup>3</sup>, S. K. Vines<sup>4</sup>, B. Hubert<sup>5</sup>, and M. R. Hairston<sup>6</sup>

<sup>1</sup>School of Physics and Astronomy, University of Leicester, Leicester, UK, <sup>2</sup>Department of Physics, Umeå University, Umeå, Sweden, <sup>3</sup>Johns Hopkins University Applied Physics Laboratory, Laurel, MD, USA, <sup>4</sup>Southwest Research Institute, San Antonio, TX, USA, <sup>5</sup>Laboratory of Planetary and Atmospheric Physics, University of Liège, Liege, Belgium, <sup>6</sup>William B. Hanson Center for Space Sciences, University of Texas at Dallas, Richardson, TX, USA

**Abstract** A necessary condition for the generation of Geomagnetically Induced Currents (GICs) that can pose hazards for technological infrastructure is the occurrence of large, rapid changes in the magnetic field at the surface of the Earth. We investigate the causes of such dB/dt events or "spikes" observed by SuperMAG at auroral latitudes, by comparing with the time-series of different types of geomagnetic activity for the duration of 2010. Spikes are found to occur predominantly in the pre-midnight and dawn sectors. We find that pre-midnight spikes are associated with substorm onsets. Dawn sector spikes are not directly associated with substorms, but with auroral activity occurring within the westward electrojet region. Azimuthally-spaced auroral features drift sunwards, producing Ps6 (10–20 min period) magnetic perturbations on the ground. The magnitude of dB/dt is determined by the flow speed in the convection return flow region, which in turn is related to the strength of solar wind-magnetospheric coupling. Pre-midnight and dawn sector spikes can occur at the same time, as strong coupling favors both substorms and westward electrojet activity; however, the mechanisms that create them seem somewhat independent. The dawn auroral features share some characteristics with omega bands, but can also appear as north-south aligned auroral streamers. We suggest that these two phenomena share a single underlying cause. The associated fluctuations in the westward electrojet produce quasi-periodic negative excursions in the AL index, which can be mis-identified as recurrent substorm intensifications.

**Plain Language Summary** Sudden changes in electrical currents flowing in the auroral ionosphere produce magnetic perturbations on the ground, large dB/dt "spikes," which can lead to damaging Geomagnetically Induced Currents (GICs) in technological infrastructure. It is known that these spikes occur preferentially in the pre-midnight local time sector and near dawn, though their exact cause is still poorly understood. In this study we show that pre-midnight spikes are associated with the well-known auroral substorm phenomenon which produces sudden southward-directed perturbations in the magnetic field. Dawn spikes are associated with east-west spaced auroral features which drift eastwards and produce wave-like fluctuations in the magnetic field in the east-west direction. The magnitude of dB/dt will depend on the speed at which the forms drift. Pre-midnight and dawn spikes are not directly related, but can occur together when geomagnetic activity is high.

#### 1. Introduction

Geomagnetically Induced Currents (GICs), which negatively impact geographically-extended power-grids and pipelines, are caused by rapid fluctuations in electrical currents flowing in the auroral ionosphere which in turn produce sudden changes in the magnetic field on the ground, also known as large dB/dt events or "spikes." These ionospheric currents are a component of the electrical circuit which transmits stress from the magnetosphere to the ionosphere as part of the Dungey cycle of convection (Dungey, 1961; Milan et al., 2017), driven by the solar wind-magnetosphere interaction. This study investigates the link between different types of geomagnetic activity and the occurrence of large dB/dt events. We identify two main hot-spots of spike occurrence, in the pre-midnight and dawn sectors, which occur for different activity types.

Disturbances of the magnetosphere are produced by the solar wind interaction, so the occurrence of large dB/dt displays dependencies on solar wind conditions and hence the solar cycle (e.g., Milan, Imber, et al., 2023). Magnetospheric activity encompasses a range of behaviors including geomagnetic storms (e.g., Gonzalez

MILAN ET AL. 1 of 16

et al., 1994), substorms (e.g., Akasofu, 1964), periods of "steady magnetospheric convection" (e.g., Sergeev et al., 1996), intervals of prolonged, repeated auroral activity, termed "multiple intensifications" (Milan et al., 2021), and "high-intensity long-duration continuous AE activity" (HILDCAA) which occurs during high-speed solar wind streams (e.g., Milan, Mooney, et al., 2023; Tsurutani & Gonzalez, 1987). Most of these phenomena have been implicated in the occurrence of dB/dt (e.g., Fleetham et al., 2024; Juusola et al., 2015; Milan, Imber, et al., 2023; Schillings et al., 2022). Different current systems will be responsible for the generation of spikes at different local times during different types of activity. Although there is still debate over exactly which phenomena are responsible, candidates include the substorm current wedge (SCW) in the pre-midnight sector, a dawn-side current wedge, omega bands in the dawn sector, and Kelvin-Helmholtz wave activity in the pre-noon sector (e.g., Apatenkov et al., 2020; Engebretson et al., 2020; Juusola et al., 2015; Kataoka & Pulkkinen, 2008; Milan, Imber, et al., 2023; Ngwira et al., 2018; Pulkkinen & Kataoka, 2006; Sorathia et al., 2023; Weigel et al., 2002, 2003; Zou et al., 2022).

Instances of large dB/dt have been shown to occur in three main local time hot-spots: the pre-midnight, dawn, and pre-noon sectors (e.g., Fleetham et al., 2024; Juusola et al., 2015; Kataoka & Pulkkinen, 2008; Milan, Imber, et al., 2023; Schillings et al., 2022; Viljanen et al., 2001; Weigel et al., 2002). Milan, Imber, et al. (2023) showed examples of magnetograms containing periods of high dB/dt from these hot-spots: in the pre-midnight sector these tend to be sudden negative excursions of the north-south component, associated with the formation of the SCW; in the dawn sector these tend to be associated with Ps6 ultralow frequency (ULF) pulsations (Rajaram et al., 1986; Rostoker & Barichello, 1980), with periods in the range 10–20 min, in both the north-south and east-west components; in the pre-noon sector they take the form of  $\sim$ 5 min ULF pulsations in all three components.

We investigate the causal mechanisms of GICs statistically by cross-referencing the occurrence of dB/dt spikes with the nature of the on-going geomagnetic activity. Milan et al. (2021) identified the sequence of different types of geomagnetic activity during the year 2010, and in this study we compare this sequence with the occurrence of spikes determined from SuperMAG ground magnetometer measurements (Gjerloev, 2012). Although 2010 was a year of low solar activity, and hence relatively weak geomagnetic activity, the ability to compare spike occurrence with convection state provides useful insights into spike formation, highlighting the difference between the causes of spikes in the pre-midnight and dawn sectors. We then further study the difference between pre-midnight and dawn spikes using two case studies from 2001, a year of high solar activity, and 2010.

#### 2. Observations

#### 2.1. Geomagnetic Activity Types

As described by Milan et al. (2021), the variation in geomagnetic activity type — or magnetospheric "convection state" — for the duration of 2010 was determined by considering the behavior of the orientation and magnitude of the interplanetary magnetic field (IMF), the auroral upper and lower electrojet indices AU and AL (Davis & Sugiura, 1966), the polar cap or PC index (Troshichev et al., 2006), and the latitude of the region 1 and 2 fieldaligned currents (FACs) measured by the Active Magnetosphere and Planetary Electrodynamics Response Experiment or AMPERE (Anderson et al., 2000; Waters et al., 2001). Solar wind and geomagnetic index data were accessed from the NASA/OMNI data set (Papitashvili & King, 2020). The latitude of the AMPERE FACs was determined by fitting a circle to the boundary between the region 1 and region 2 currents (Milan, 2019; Milan et al., 2015), of which the radius, A, was used as a proxy for the open or polar cap flux content of the magnetosphere,  $F_{PC}$ . Convection state is largely determined by the occurrence of dayside (magnetopause) reconnection and nightside (magnetotail) reconnection, quantified by  $\Phi_D$  and  $\Phi_N$ , which can occur together or independently (Cowley & Lockwood, 1992; Milan et al., 2007), as shown in Figure 1 of Milan, Mooney, et al. (2023). Reconnection rates are difficult to measure directly (Chisham et al., 2008; Hubert et al., 2006), so a proxy for  $\Phi_D$ based on upstream solar wind speed and the interplanetary magnetic field (IMF),  $\Phi_D^*$ , is used (Milan et al., 2012). The data was analyzed by eye and the following activity types were identified by Milan et al. (2021) (more details can be found in that paper):

- Quiet: little or no geomagnetic activity;
- · Weak Activity: geomagnetic activity but with no substorm or other signatures;
- Substorm Growth Phase: unbalanced dayside reconnection causing an expansion of the polar cap, that is, IMF  $B_Z < 0$ , increasing  $F_{PC}$  and AU/AL;

MILAN ET AL. 2 of 16

onlinelibrary.wiley.com/doi/10.1029/2024JA032811 by Southwest Research Institute, Wiley Online Library on [02/04/2025]. See the Terms

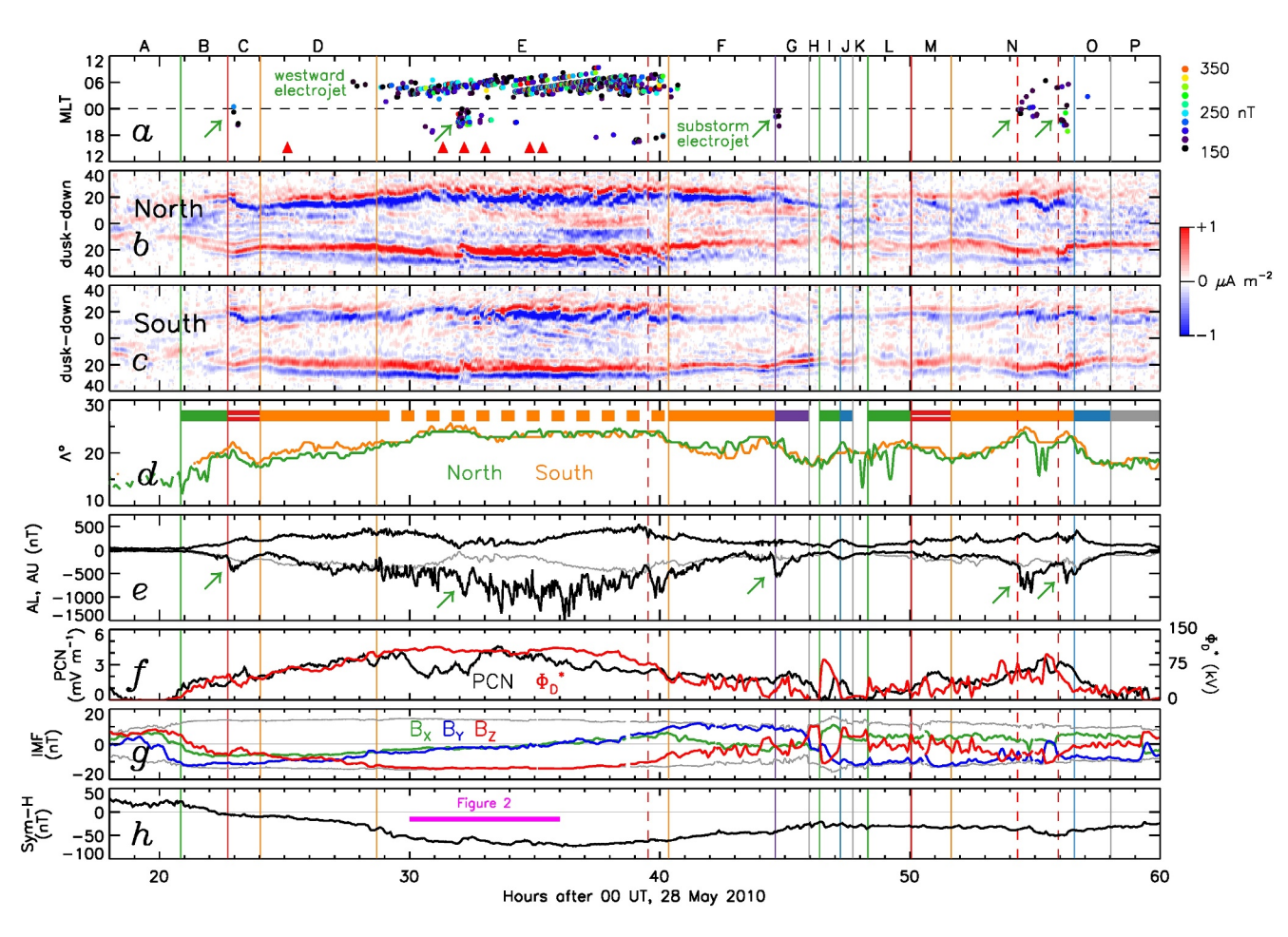


**Figure 1.** Spike occurrence and context on the 28–30 May 2010. Panel a: the MLT occurrence of dB/dt > 150 nT min<sup>-1</sup>. Panels b and c: AMPERE observations of field-aligned currents (FACs) along the dusk-dawn meridians of the northern and southern hemispheres; dawn is toward the top in each case. Panel d: the radii,  $\Lambda$ , of the FAC rings in the two hemispheres. Panel e: the AU and AL indices. Panel f: the PC-N index and  $\Phi_D^*$ . Panel g: the  $B_X$ ,  $B_Y$ , and  $B_Z$  components of the interplanetary magnetic field. Panel h: the Sym-H index. Greens arrows in panels a and e highlight the onset of substorms. A magenta bar in panel h indicates the time interval covered by Figure 2.

- Substorm Expansion Phase: a substorm bay (negative excursion) in the AL index;
- Substorm Driven Phase: balanced dayside and nightside reconnection leading to steady magnetospheric convection, that is, IMF  $B_Z < 0$  but uniform  $F_{PC}$  and enhanced AU/AL;
- Substorm Recovery Phase: unbalanced nightside reconnection leading to a contraction of the polar cap, that is, IMF  $B_Z > 0$ , decreasing  $F_{PC}$  and AU/AL;
- Recovery Bay: recovery phases accompanied by a substorm-like bay in AL;
- Multiple Intensifications: prolonged, rapid quasi-periodic variations in AL, usually during strong solar wind driving, and associated with an expanded auroral oval.

Examples of these activity types are presented in Figure 1, which shows a period of 42 hr of observations from 18 UT on 28 May 2010. Panels b and c show cuts of AMPERE-derived FAC density along the dawn-dusk meridian in the northern and southern hemispheres, color-coded with red and blue as upwards and downwards FACs, respectively. Panel d shows the radius of the FACs,  $\Lambda$ , in the northern and southern hemispheres. Panel e shows the AU and AL indices, f the PC-N index and  $\Phi_D^h$ , g the components of the IMF, and h the Sym-H index.

Vertical lines show the boundaries between different convection states, and letters at the top label these intervals. A, H, and K are quiet. B, I, and L are growth phases ( $\Phi_D > 0$ ,  $\Lambda$  increasing). C and M are expansion phases (substorm bay in AL, often accompanied by a decrease in  $\Lambda$ ). D, F, and N are driven phases ( $\Phi_D > 0$  but steady  $\Lambda$  indicating  $\Phi_N \approx \Phi_D$ ). J and O are recovery phases ( $\Phi_D \approx 0$  but  $\Lambda$  decreasing indicating  $\Phi_N > 0$ ). G is a recovery bay (a recovery phase but with a substorm bay in AL) and P is a period of weak activity. Vertical red dashed lines

MILAN ET AL. 3 of 16

during intervals E and N identify events that were termed driven phase onsets by Milan et al. (2021). Driven phases are periods of balanced dayside and nightside reconnection, and driven phase onsets are a new substorm onset — presumably associated with the formation of a new near-Earth neutral line and development of a new substorm current wedge (Milan et al., 2021) — during already ongoing magnetotail reconnection. Interval E is the type of activity identified as multiple intensifications by Milan et al. (2021), due to the rapid fluctuations in AL, and is of especial interest to the present study. The 10–20 min quasi-periodic fluctuations in AL are manifestly different from the substorm growth/expansion behavior of states B and C, where a substorm cycle typically lasts 3 hr, and the driven onsets in intervals E and N. True substorm bays in AL are highlighted by green arrows in panel *e*.

In total, for the year 2010, almost 3,500 consecutive periods of different activity were found, including 752 growth phases, 568 substorm onsets, 447 driven phases, 502 recovery phases, and 12 periods of multiple intensifications. This data set is available as Milan (2020).

#### 2.2. Identifying dB/dt Spikes

One-minute cadence ground magnetometer data were accessed via the SuperMAG repository (Gjerloev, 2012). The data have the background field subtracted and are then rotated into N (North-South, positive northwards), E (East-West, positive eastwards), and E (vertical, positive downwards) components. As described by Schillings et al. (2022) and Milan, Imber, et al. (2023), dB/dt was defined as the minute-on-minute difference between successive E0, E1, and E2 values, denoted E2. We use E3 to denote a difference in any field component. Molinski et al. (2000) identified E3 E4 as a threshold for producing harmful GICs, which equates to E4 and E5 E6 are the successive values of E8 and E9 and E9 and E9 are the successive values of E9.

Figure 2 shows N, E, and Z magnetograms from eight SuperMAG stations between 06 and 12 UT on 29 May 2010 (i.e., coinciding with a portion of Figure 1, indicated by the horizontal bar in panel h). Four stations traverse the pre-midnight sector (left column) and four the dawn sector (right column) during this period. Fluctuations in the field measurements are quantified by  $\Delta B$  in the minute-cadence data and converted into dB/dt, presented superimposed from all four stations in the lower panels. In the left column, all four stations see a negative excursion in N around 08 UT, producing negative spikes in  $\Delta N$  close to -300 nT min<sup>-1</sup>, equivalent to  $|dB/dt| \approx 5$  nT s<sup>-1</sup>. This is a substorm onset. In the right column, all stations see quasi-periodic fluctuations in mainly the N and E components, with associated |dB/dt| values exceeding 10 nT s<sup>-1</sup>. As will be discussed below, these are the signatures of omega bands and similar eastward-traveling features in the dawn sector auroral zone. The easternmost station, NAQ, sees these fluctuations near the start of the interval, whereas the western-most station, FCC, sees them toward the end. This indicates that the dawn sector activity is on-going throughout this period, and that the stations rotate under the activity as the day progresses. This is in contrast to the substorm in the pre-midnight sector, in which spike activity is confined to a relatively short duration around 08 UT. Close examination of individual spikes in  $\Delta B$  show that they tend to have durations of 1–2 min, both in the pre-midnight sector and at dawn.

To identify spikes, we threshold  $|\Delta B|$  at various levels. Bearing in mind that  $|\Delta B|$  likely underestimates |dB/dt|, and that 2010 is a year of low solar activity, we use a threshold of  $|\Delta B| > 250 \,\mathrm{nT}\,\mathrm{min}^{-1}$  for our statistical survey of spike occurrence in Section 2.3. When we conduct case studies in Section 2.4, we use a lower threshold of  $|\Delta B| > 150 \,\mathrm{nT}\,\mathrm{min}^{-1}$  as this allows us to investigate the relationship between spikes occurring in the pre-midnight and dawn sectors. For instance, the occurrence and MLT location of such spikes during the interval encompassed by Figure 1 (and Figure 2) is shown in Figure 1a.

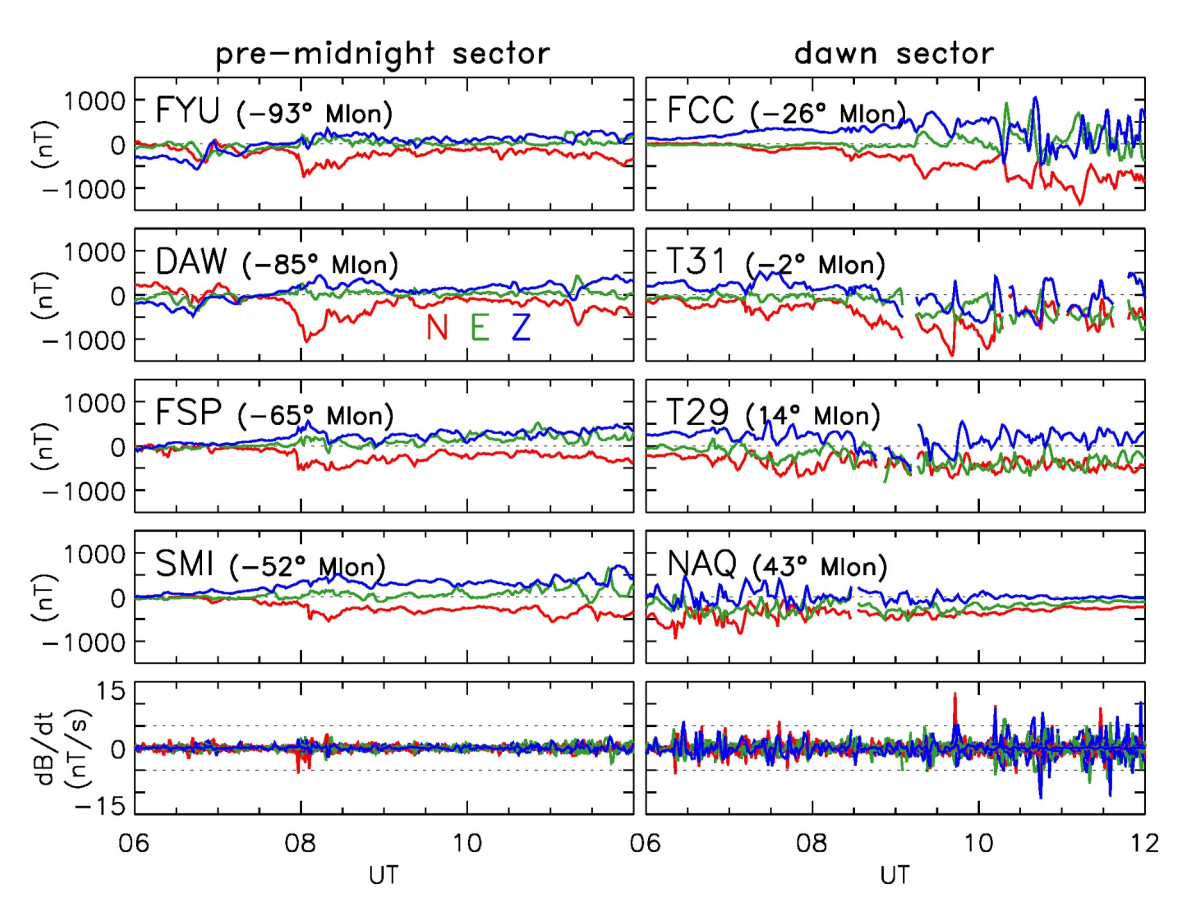
#### 2.3. Statistical Study of Spike Occurrence for 2010

Figure 3 presents the magnetic local time (MLT) and magnetic latitude of spikes with  $|\Delta B| > 250$  nT occurring during the growth, expansion, driven, multiple intensifications, recovery, and recovery bay convection states of 2010. Very few spikes are observed during the quiet and weak activity states, so these are omitted. In each panel, the name of the state is followed by the percentage of time that the magnetosphere spent in that state during 2010. The number of spikes identified in each state is shown, along with the percentage of all spikes that this number represents. Finally, the rate of occurrence of spikes during that state is shown as the number of spikes per day.

MILAN ET AL. 4 of 16

21699402, 2024, 10, Downlo

onlinelibrary.wiley.com/doi/10.1029/2024JA032811 by Southwest Research Institute, Wiley Online Library on [02/04/2025]. See the Terms



**Figure 2.** SuperMAG magnetometer measurements from 8 stations located primarily in the pre-midnight sector (left column) and dawn sector (right column) on 29 May 2010. From top to bottom in each column the stations are shown in order of increasing magnetic longitude. The bottom panels show dB/dt from the four upper panels all superimposed, with horizontal dotted lines indicating  $\pm 5$  nT s<sup>-1</sup>.

Each occurrence of a spike is indicated by a colored dot. The color-coding represents whether the spikes tended to occur near the start, near the end, or in the middle of each convection state ("elapsed time"). A polar histogram in each panel shows the occurrence distribution of spikes in 1 hr wide MLT bins, on the logarithmic scale shown in the bottom right panel.

Overall, spikes occur in two distinct MLT ranges, which we refer to as the pre-midnight (19–00 MLT) and dawn (03-07 MLT) sectors. These well-known "hot-spots" have previously been identified by a number of authors (e.g., Juusola et al., 2015; Kataoka & Pulkkinen, 2008; Milan, Imber, et al., 2023; Schillings et al., 2022; Viljanen et al., 2001; Weigel et al., 2002). Here we show that the occurrence of these hot-spots is strongly dependent on convection state. Few spikes are observed during the growth phase (2.4% of the total); those that are observed tend to occur late in the growth phase, so are probably associated with the subsequent expansion phase. A more significant number of spikes (16.9%) is seen in the expansion phase, and usually near the start of this phase, suggesting that they are associated with substorm onset. These are concentrated in the 21 to 00 MLT sector, implying that they are caused by the westward electrojet component of the substorm current wedge. More spikes (19.8%) are seen during the driven phase, with no preference for the elapsed time. These are mainly observed in the pre-midnight sector, but with a small number at dawn. Most of the pre-midnight spikes will be associated with driven phase onsets. The majority of spikes (54.2%) are observed during multiple intensifications, in both the premidnight and dawn sectors, but concentrated in the dawn sector (76% in the 01-07 MLT sector as opposed to 23% in the 17-00 MLT sector). Few spikes are seen during recovery phases (1.7%), but there is a small number of spikes associated with recovery bays (3.9%), almost exclusively in the pre-midnight sector. Our main conclusion is that pre-midnight spikes are associated with substorms while dawn spikes are strongly correlated with the multiple intensifications convection state identified by Milan et al. (2021). Although negative excursions in AL are usually assumed to be associated with substorm activity in the pre-midnight sector, in these cases they are

MILAN ET AL. 5 of 16

21699402, 2024, 10, Downloaded from https://agupubs.onlinelibrary.wiley.com/doi/10.10292024J.0032811 by Southwest Research Institute, Wiley Online Library on [02/04/2025]. See the Terms and Conditions (https://onlinelibrary.wiley.com/

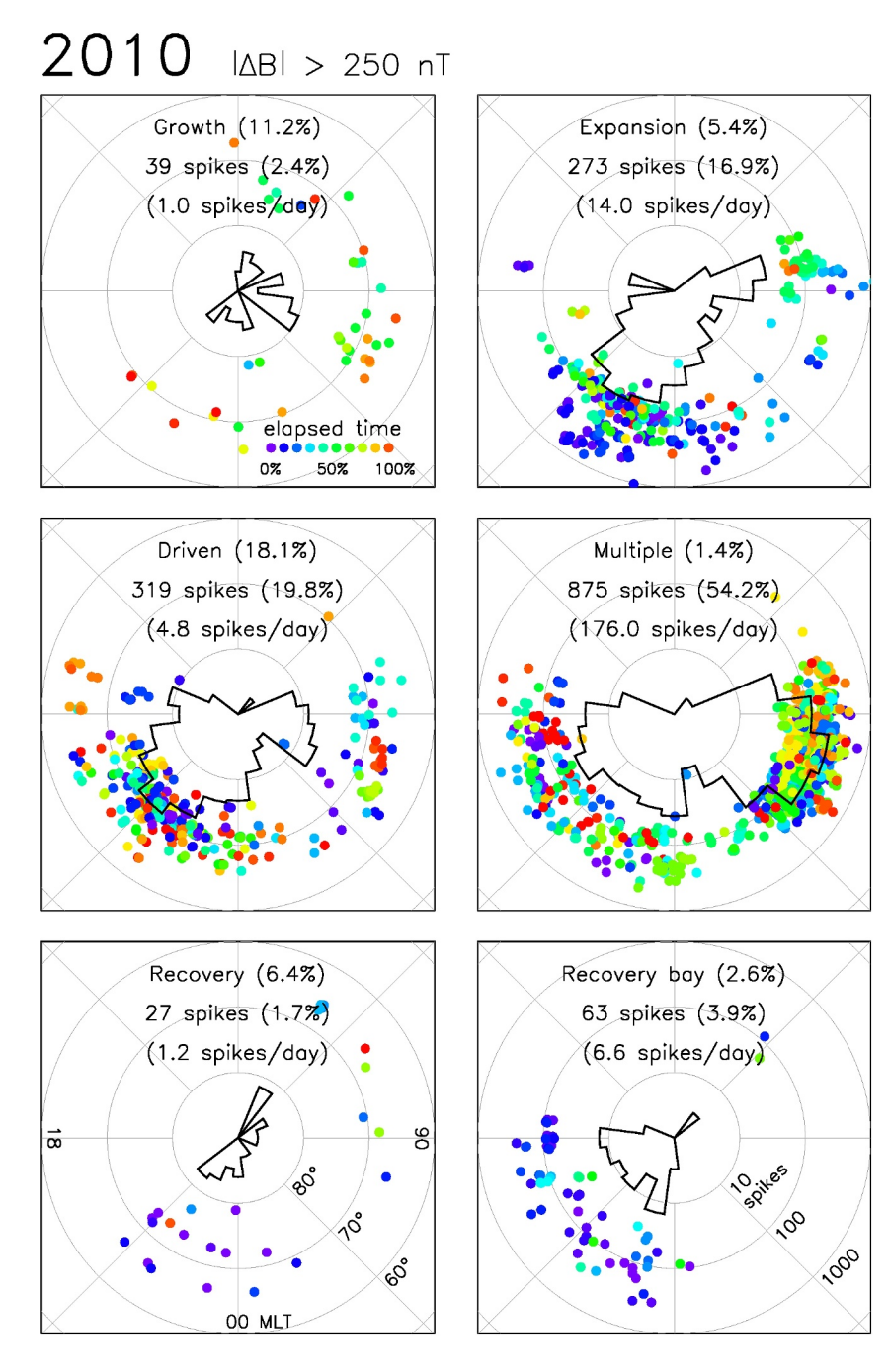


Figure 3. Magnetic local time and magnetic latitude occurrence distribution of  $dB/dt > 250 \text{ nT min}^{-1}$  during different convection states in 2010. Noon is to the top and dawn to the right; gray circles indicate magnetic latitudes in steps of 10°. The events are color-coded by their time of occurrence within each state. A polar occurrence histogram is shown within each panel, on the logarithmic scale shown in the bottom-right panel.

caused by westward electrojet activity in the dawn sector. Moreover, while multiple intensifications occupy less than 2% of the time, they produce over 54% of spikes.

We now focus on spikes with  $|\Delta B| > 250$  nT occurring during expansion phase, driven phase, multiple intensifications, and recovery bays. The distributions of spikes during these states are presented in Figure 4, this time color-coded with respect to spike magnitude ( $|\Delta B|$ ), the spike component (N, E, or Z), dayside reconnection rate ( $\Phi_D^*$ ), solar wind speed ( $V_{SW}$ ), IMF  $B_Z$ , and the Sym-H index (Iyemori, 1990). We tried different methods to

MILAN ET AL. 6 of 16

2169402, 2024, 10, Downloaded from https://agupubs.onlinelibrary.wiley.com/doi/10.1029/2024/A032811 by Southwest Research Institute, Wiley Online Library on [02/04/2025]. See the Terms and Conditions (https://onlinelibrary.wiley.com/doi/10.1029/2024/A032811 by Southwest Research Institute, Wiley Online Library on [02/04/2025]. See the Terms and Conditions (https://onlinelibrary.wiley.com/doi/10.1029/2024/A032811 by Southwest Research Institute, Wiley Online Library on [02/04/2025]. See the Terms and Conditions (https://onlinelibrary.wiley.com/doi/10.1029/2024/A032811 by Southwest Research Institute, Wiley Online Library on [02/04/2025]. See the Terms and Conditions (https://onlinelibrary.wiley.com/doi/10.1029/2024/A032811 by Southwest Research Institute, Wiley Online Library on [02/04/2025]. See the Terms and Conditions (https://onlinelibrary.wiley.com/doi/10.1029/2024/A032811 by Southwest Research Institute, Wiley Online Library on [02/04/2025]. See the Terms and Conditions (https://onlinelibrary.wiley.com/doi/10.1029/2024/A032811 by Southwest Research Institute, Wiley Online Library on [02/04/2025]. See the Terms and Conditions (https://onlinelibrary.wiley.com/doi/10.1029/2024/A032811 by Southwest Research Institute, Wiley Online Library on [02/04/2025]. See the Terms and Conditions (https://onlinelibrary.wiley.com/doi/10.1029/2024/A032811 by Southwest Research Institute (https://onlinelibrary.wiley.com/doi/10.1029/2024/A032811 by Southwest Research (https://onlinelibrary.wiley.c

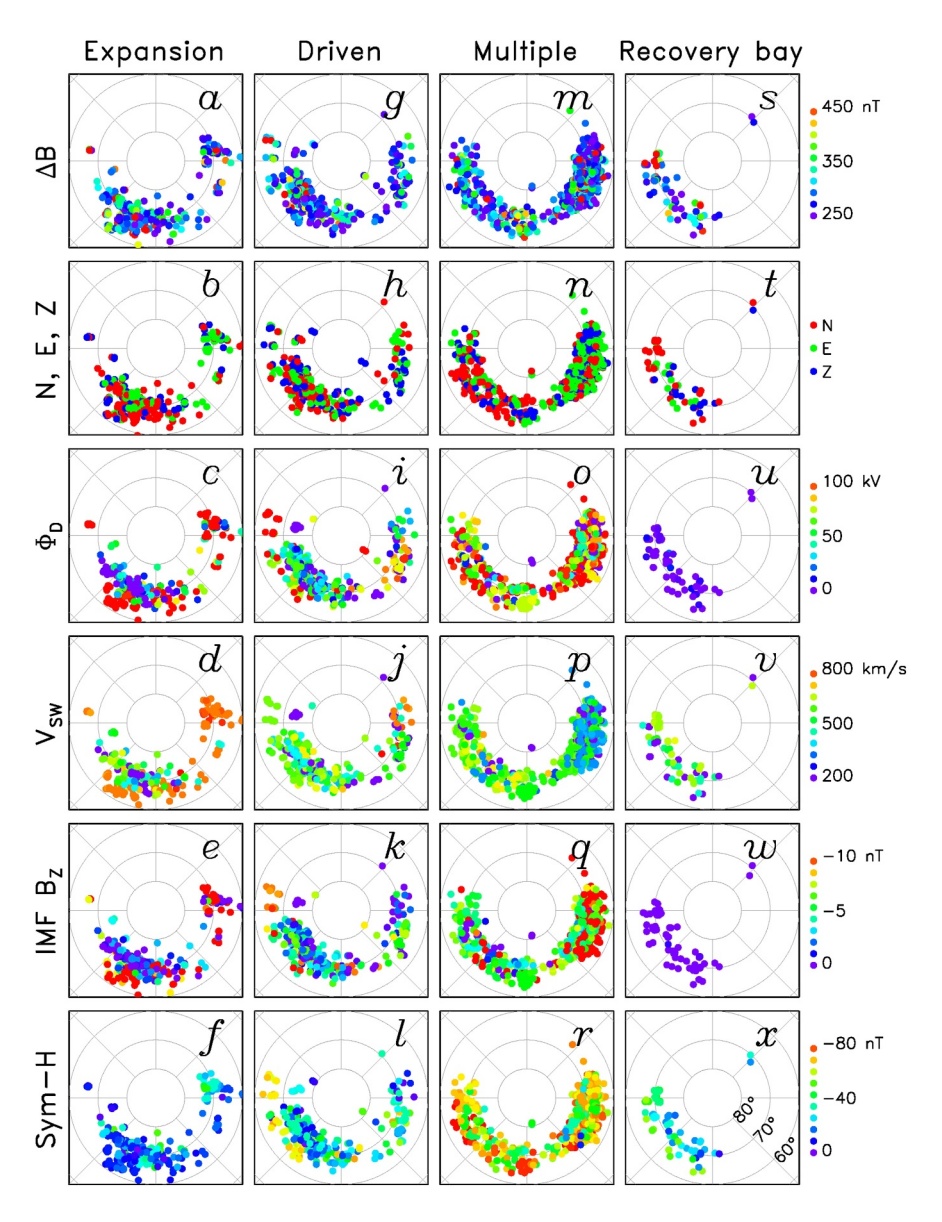


Figure 4. Occurrence distribution of  $dB/dt > 250 \text{ nT min}^{-1}$  in a similar format to Figure 3. The color-coding refers to the magnitude of dB/dt,  $\Delta B$ , the component in which  $\Delta B$  occurs, reconnection rate  $\Phi_D^{\star}$ , solar wind speed  $V_{SW}$ , IMF  $B_Z$ , and the Sym-H index.

compare spike times with respect to the OMNI solar wind data: using instantaneous values of the solar wind parameters, or averaging the solar wind for 30 min or 1 hr prior to the spike time. Each method made very little difference to the distributions, so here we show the instantaneous values. That averaging made no difference suggests that spikes often occur during periods of steady solar wind.

Spike magnitude does not appear to be strongly dependent on convection state nor local time (panels a, g, m, s). Magnitudes range from the threshold, 250 nT, up to 450 nT, though with fewer at higher values. (Bear in mind that 2010 was a quiet year and we would expect larger spikes in more active years.) Spikes in all three components can occur in all states at all MLTs, though N spikes are favored in the pre-midnight sector and E spikes at dawn (panels b, h, n, t), as previously reported (e.g., Milan, Imber, et al., 2023; Schillings et al., 2022).

During expansion phase most spikes occur in the pre-midnight and midnight sectors, mainly between 21 and 02 MLT. These occur predominantly for non-storm times, typically Sym-H >  $-20 \,\mathrm{nT}$  (panel h), though they occur at lower latitudes for high  $V_{SW}$  and more negative IMF  $B_Z$ , and hence also for high  $\Phi_D^*$  (panels c, d, e). A secondary

MILAN ET AL. 7 of 16

21699402, 2024, 10, Dow

population at 06 to 08 MLT is seen during expansion phases. The most notable aspect of these is that they occur for high  $V_{SW}$  (panel d), so they resemble the Kelvin-Helmholtz instability spike population described by Weigel et al. (2003) and Milan, Imber, et al. (2023). It is unclear if it is a coincidence that this population appears during expansion phases only (though there is a hint of this high- $V_{SW}$  population during driven phases (panel j) also).

Most driven phase spikes occur in the pre-midnight sector, mainly between 19 and 01. This MLT distribution is perhaps shifted to slightly earlier local times than the expansion phase population. These spikes appear at lower latitudes for elevated Sym-H  $\approx$  -60 nT and  $\Phi_D^{\star} \approx$  100 kV (panels l and i, respectively).

The multiple intensification spikes occur at pre-midnight and dawn, though mainly dawn as described above. This convection state occurs during strong driving (Milan et al., 2021), and as a consequence Sym-H tends to be elevated, Sym-H < -40 nT (panel r). However, there are distinct differences in the solar wind conditions for the pre-midnight and dawn populations: pre-midnight spikes are favored by faster solar wind but lower values of  $B_Z$ , whereas dawn spikes occur for moderate  $V_{SW}$  but more negative  $B_Z$  (panels p and q).

Finally, recovery bay spikes, being a recovery phase phenomenon, occur for low values of  $\Phi_D^{\star}$ , moderate solar wind speed ( $\approx 500 \text{ km s}^{-1}$ ) and slightly elevated Sym-H  $\approx -40 \text{ nT}$  (panels u, v, x). These spikes occur between 18 and 00 MLT, a somewhat different distribution than the substorm onset spikes. It is still unclear what leads to recovery bays (Milan et al., 2021).

#### 2.4. Two Case Studies of Pre-Midnight and Dawn Spikes

#### 2.4.1. 28-30 May 2010

We now refer back to Figure 1, in which panel a shows the MLT location of spikes with  $|\Delta B| > 150$  nT. In this example, highlighted by green arrows, weak spikes are seen in the pre-midnight sector associated with the expansion phase C, with the recovery bay G, and with the two driven phase onsets indicated by vertical red dashed lines during interval N. However, the majority of spikes are seen in the dawn sector during state E. A cluster of spikes is also seen in the pre-midnight sector at 32 hr, highlighted by a further green arrow, which is associated with a substorm onset occurring during the ongoing period of dawn activity (the corresponding magnetograms are presented in Figure 2). Green arrows in panel e highlight the substorm bays in AL that are associated with the pre-midnight activity; other fluctuations in AL are produced by dawn sector activity.

Panel c shows that the southern hemisphere duskside region 1 and 2 FAC system (Iijima & Potemra, 1976) is steady during interval E, except for the substorm onset at 32 hr, whereas the dawnside R1/R2 system fluctuates in intensity and location. Panel b shows the same for the northern hemisphere, but with even more structure apparent at dawn, and some variability at dusk as well after 37 hr. We note that some weak spike activity is seen between 37 and 40 hr in the dusk sector, recorded in the northern hemisphere, which may be associated with the duskside R1/R2 fluctuations.

We now investigate the auroral and FAC signatures associated with the spikes seen during intervals D and E of Figure 1. Auroral observations are provided by the Special Sensor Ultraviolet Spectrographic Imager (SSUSI) experiment (Paxton et al., 1992) onboard the Defense Meteorological Satellite Program (DMSP) F16 and F18 satellites. The DMSP satellites are in sun-synchronous orbits roughly aligned with the dawn-dusk meridian near an altitude of 850 km. SSUSI recorded a swath of auroral luminosity, extending sunwards and antisunwards from the orbit, in five wavelength bands. We use observations at 121.6 nm, which measures Lyman– $\alpha$  emissions associated with proton precipitation, and the Lyman-Birge-Hopfield short (LBHs) band, 140–152 nm, sensitive to emissions produced by soft electron precipitation.

Figure 5 presents six passes of the DMSP F16 or F18 spacecraft over the northern or southern hemispheres, the times of which are indicated by red arrows in Figure 1a. Most passes are from the southern hemisphere to optimize viewing of the dawn sector auroral oval, though the coverage of SuperMAG is better in the northern hemisphere. For each pass we also show the concurrent FAC distribution from AMPERE in both hemispheres. Superimposed on the AMPERE panels, cyan circles show the occurrences of spikes within  $\pm 7$  minutes of the midpoint of the pass (covering the approximate duration of the pass), where the circle radii indicate the magnitudes of the spikes.

The first pass occurs during driven phase D. The auroras are relatively featureless, and the FACs have the characteristic R1/R2 structure (Iijima & Potemra, 1976) associated with standard twin-cell ionospheric

MILAN ET AL. 8 of 16

2169902, 2024, 10, Downloaded from https://agupubs.onlinelibrary.wiley.com/doi/10.1029/2024/A032811 by Southwest Research Institute, Wiley Online Library on [02/04/2025]. See the Terms and Conditions (https://onlinelibrary.wiley.com/ems-and-conditions) on Wiley Online Library for rules of use; OA articles are govern

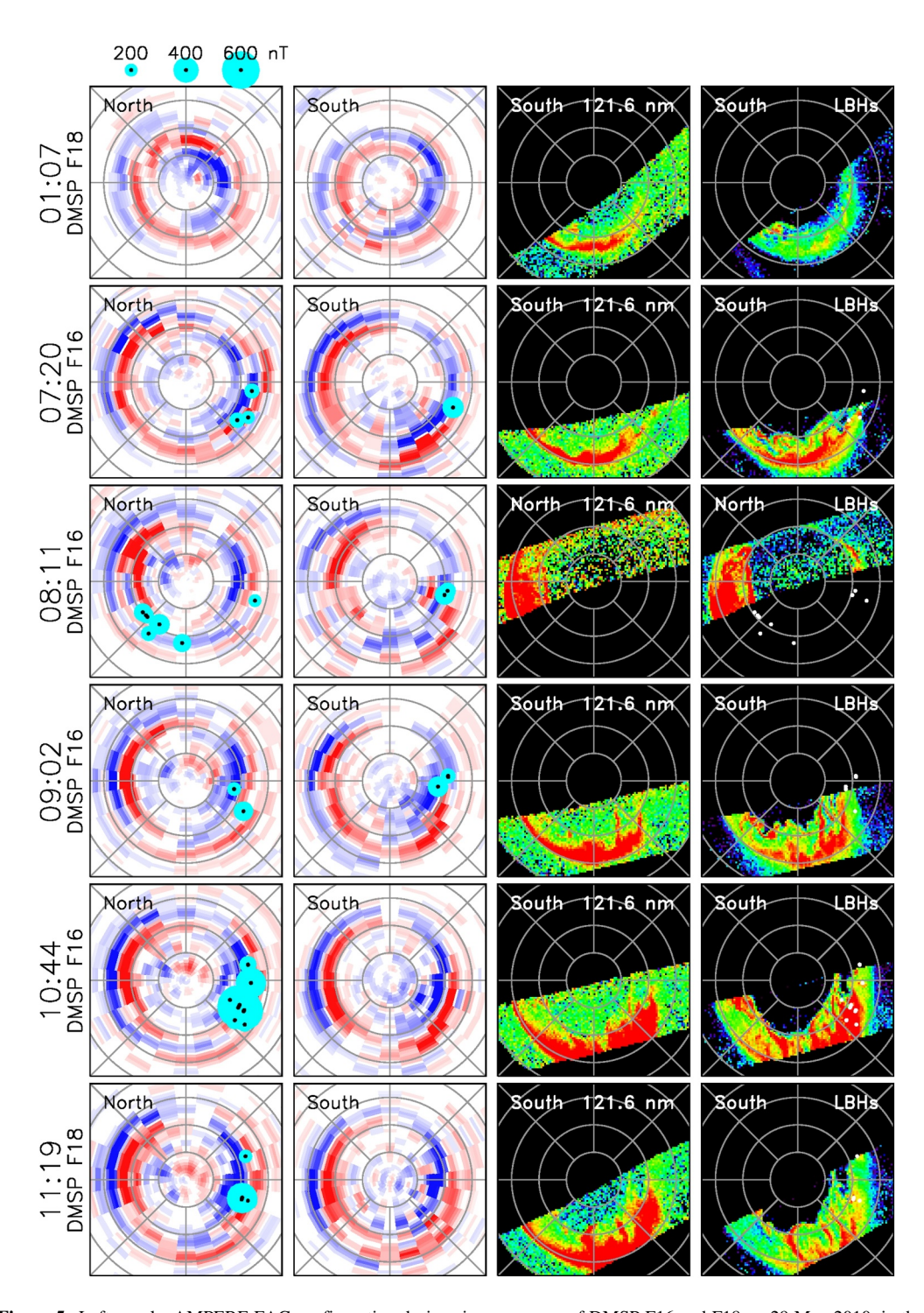


Figure 5. Left panels: AMPERE FAC configuration during six overpasses of DMSP F16 and F18 on 29 May 2010, in the northern and southern hemispheres. Noon is to the top and dawn to the right of each panel. Cyan circles show the occurrence of  $dB/dt > 200 \,\mathrm{nT}$  min<sup>-1</sup> in each hemisphere during the duration of each overpass. Right panels: DMSP/SSUSI observations of 121.6 nm and LBHs emissions in each overpass.

convection. No spikes are observed at this time. The other passes occur during the period of multiple intensifications, interval E. The first is prior to the substorm onset at 32 hr. The auroras have brightened and the FACs have gained a more complicated structure, especially at dawn. Spikes in excess of 200 nT are seen in the dawn sector of both hemispheres at this time. The third pass occurs during the onset at 32 hr. The auroras have

MILAN ET AL. 9 of 16

expanded to lower latitudes and are much brighter, with a prominent westward-traveling surge seen at dusk, associated with a strong upwards FAC region. Spikes are seen both at dawn and in the pre-midnight substorm onset location. In the fourth pass, streamer-like auroral forms have developed in the dusk sector oval, which has considerably broadened in latitudinal width. These streamers cover between 15° and 20° of latitude from the poleward edge of the oval to the equatorward, most bright edge. Spikes are observed in the dawn sectors of both hemispheres at this time. The streamer-like activity is even more pronounced in the fifth and sixth passes, with many intense spikes seen especially in the northern hemisphere during the fifth pass. The lack of spikes in the southern hemisphere at these times is due to a gap in the location of magnetometers.

Despite the coverage with magnetometers being better in the northern hemisphere and the DMSP orbits favoring viewing of the dawn sector auroras in the southern hemisphere, we assume that there is interhemispheric conjugacy in the streamer/spike phenomena. The streamers are associated with complicated FAC structures, which are beyond the temporal and spatial resolution of AMPERE to resolve accurately. However, there is evidence for quasi-periodic behavior in the FACs on timescales of 20–30 min (see Figures 1b and 1c).

#### 2.4.2. 20 March 2001

To investigate the dynamics of the auroral features with higher temporal resolution than available with DMSP, we searched for similar observations during the mission lifetime (2000–2005) of the Imager for Magnetopause-to-Aurora Global Explorer (IMAGE), and many examples were found. IMAGE carried the FUV Wide-band Imaging Camera (WIC) instrument (Mende et al., 2000), which mainly measured LBH auroral emissions between 140 and 190 nm produced by precipitating electrons, at 2 min cadence. One such event, from 20 March 2001, is presented in Figure 6. Six snapshots from the WIC camera of the auroras in the northern hemisphere are shown in panels i to vi, with noon to the left, midnight to the right, and dawn to the top. Panels a and b show the auroral intensity as a function of MLT at magnetic latitudes of  $68^{\circ}$  and  $63^{\circ}$ , respectively; dayglow obscures the auroras near noon. Panel c shows the occurrence of spikes  $|\Delta B| > 150$  nT, panel d shows AU and AL, and panel e shows the dayside reconnection rate.

Auroral intensifications are seen in the pre-midnight sector around 01, 09, and 14 UT (panel a, green arrows), associated with substorm onsets seen in AL (panel d, green arrows). Spikes are seen in the pre-midnight sector associated with the substorms at 09 and 14 UT (panel c, green arrows). A small number of spikes are seen in the midnight sector near 01 UT associated with substorm onset at that time. Another group of spikes after 06 UT suggests an additional substorm onset at this time, when auroral observations were not available, which was also not captured by AL.

Dawn sector auroral structures, periodically-spaced in MLT, are associated with the substorm at 01 UT, highlighted by a red arrow in panel a and visible in panel i between 04 and 07 MLT. The features are separated by close to 1 hr of MLT and propagate sunwards at a speed of approximately 250 m s<sup>-1</sup> for 90 min after onset. Bursts of similar features are seen in the dawn sector almost continuously between 09 and 19 UT. Although substorms occur at 09 and 14 UT, the dawn sector activity continues long after each substorm breakup has ceased, such that the two phenomena may be largely independent. Between 09 and 19 UT the features propagate sunwards much more rapidly than at 01 UT. One burst is highlighted by a red arrow near 12 UT in panel a; the corresponding images are shown in panels ii to vi at 2 min cadence, with one auroral feature identified by arrows to indicate the motion. The features are again separated by 1 hr of MLT but propagate with a speed near 1 km s<sup>-1</sup>, giving a periodicity of approximately 10–15 min at a fixed MLT.

Figure 6c shows that significant spike activity is seen in the dawn sector, corresponding to the rapid sunward propagating auroral forms between 04 and 19 UT. Spikes are not seen at 01 to 02 UT associated with the slowly propagating features. Similar to the interval presented in Figure 1a, dawn spikes and substorms occur somewhat independently of each other. Similarly, during the interval of dawn spikes, the AL index has the characteristic variability associated with the multiple intensifications convection state. During this time  $V_{SW} \approx 400 \text{ km s}^{-1}$  and  $B_Z \approx -17 \text{ nT}$ , similar again to the conditions in Figure 1, and consistent with the statistics presented in Figure 4.

Figure 7 reproduces the IMAGE/WIC snapshot from 12:23 UT in panels *i* to *iv*. On panel *ii* is superimposed the location of SuperMAG stations which observe spikes at this time, and these are colocated with the propagating auroral features. Panels *iii* and *iv* have superimposed cross-track convection flows measured by the Ion Driftmeter (IDM) component of the Special Sensors–Ions, Electrons, and Scintillation thermal plasma analysis package or

MILAN ET AL. 10 of 16

21699402, 2024, 10, Downle

aded from https://agupubs.onlinelibrary.wiley.com/doi/10.1029/2024/A032811 by Southwest Research Institute, Wiley Online Library on [02/04/2025]. See the Terms and Conditions (https://onlinelibrary.wiley.com/

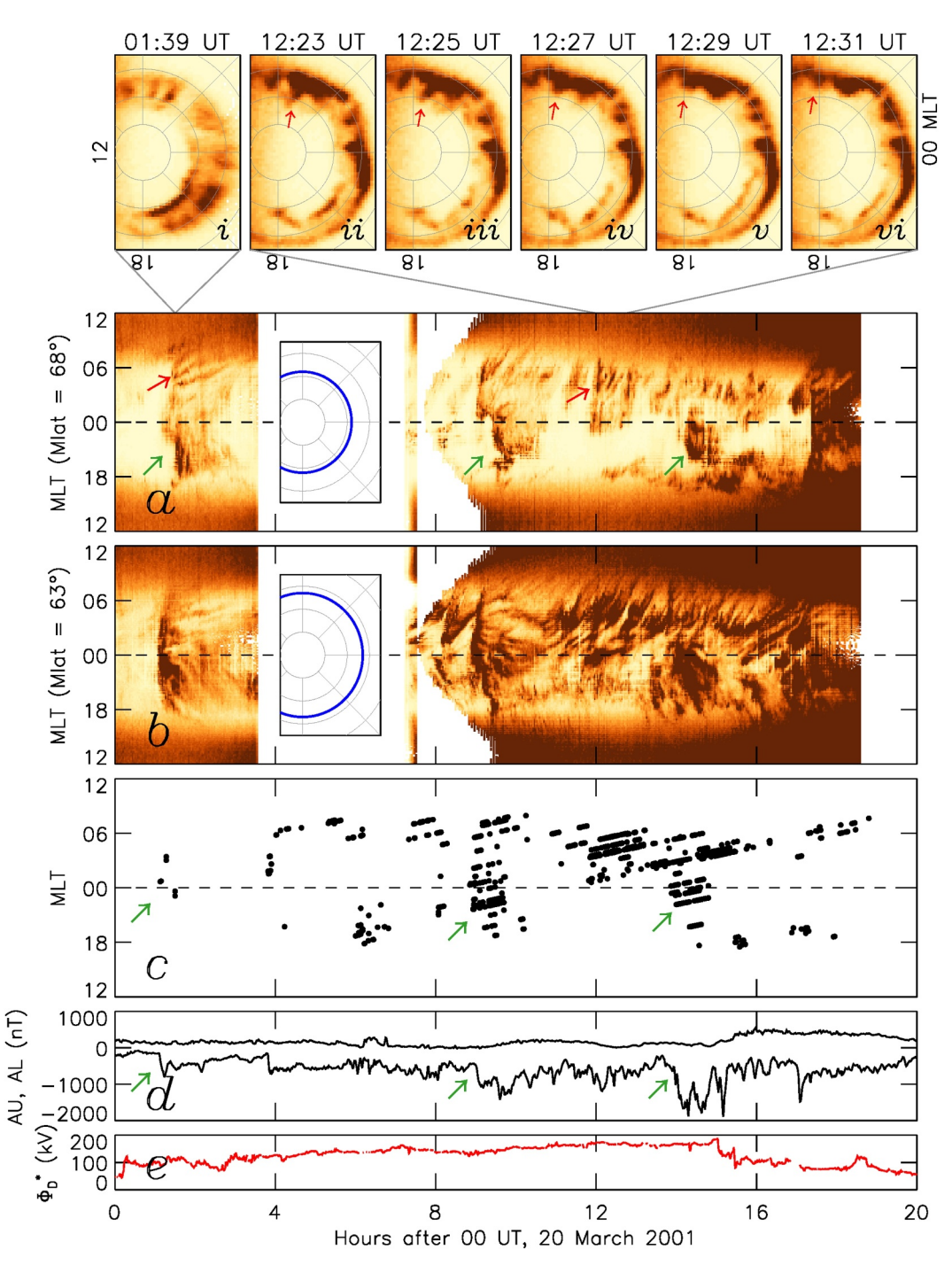
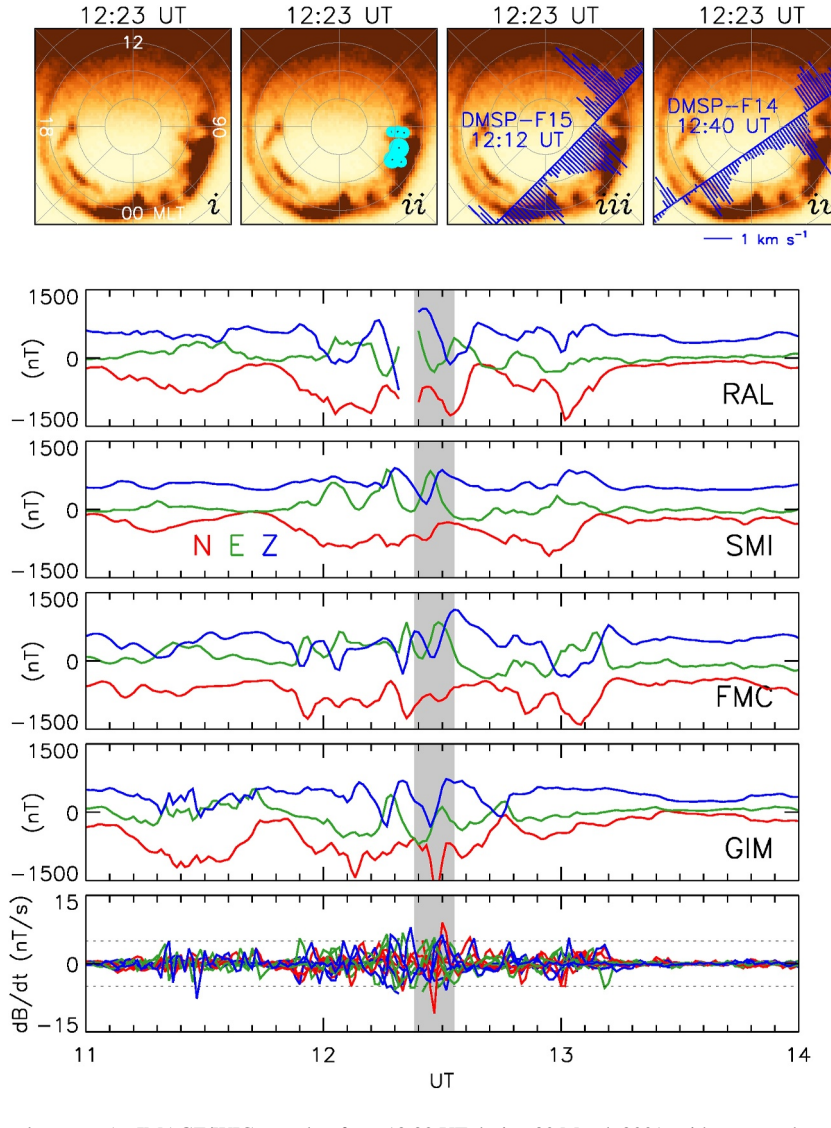


Figure 6. IMAGE/WIC auroral observations in the northern hemisphere during 20 March 2001. Panels i to vi: individual snapshots of the WIC auroral emissions, with noon to the left, dawn to the top, and midnight to the right. Red arrows track the motion of s ingle dawnside auroral feature. Panels a and b: the MLT distribution of auroral emissions at  $68^{\circ}$  and  $63^{\circ}$  magnetic latitude; auroras in the noon sector are obscured by dayglow. The inset panels show the latitude from which the MLT distribution is formed. Red arrows indicate the times of panels i and ii - vi. Panel c: the occurrence of dB/dt > 150 nT min<sup>-1</sup>. Panel d: the AU and AL indices. Panel e: the reconnection rate  $\Phi_D^{\star}$ . Green arrows in panels a, c, and d highlight the times of substorm onsets.

SSIES (Rich & Hairston, 1994) on DMSP-F15 and -F14, respectively. These two passes bracket the time sequence shown in panels *ii* to *vi* in Figure 6, showing a consistent convection pattern. Although the two passes are in the southern hemisphere, they clearly show that the auroral features are in the convection return flow region, in which

MILAN ET AL. 11 of 16

21699402, 2024, 10, Downloaded from https://agupubs.onlinelibrary.wiley.com/doi/10.1029/2024/A032811 by Southwest Research Institute, Wiley Online Library on [02/04/2025]. See the Terms and Conditions (https://onlinelibrary.wiley



**Figure 7.** Panels i to iv: An IMAGE/WIC snapshot from 12:23 UT during 20 March 2001, with noon at the top and dawn to the right. Panel ii: The location of spikes observed by SuperMAG stations during this 2-min exposure. Panels iii and iv: Cross-track convection measurements from DMSP/IDM onboard F15 and F14, respectively. Lower panels: SuperMAG magnetometer measurements from four stations located in the dawn sector; the bottom panel shows dB/dt for all four stations superimposed with horizontal dotted lines indicating  $\pm 5 \text{ nT s}^{-1}$ . The gray region highlights the period presented in Figure 6 panels ii to vi.

the flow speed is approximately  $1 \text{ km s}^{-1}$  sunwards. This speed is commensurate with the eastwards drift of the auroral features.

The lower panels of Figure 7 show magnetic measurements from a subset of SuperMAG stations colocated with the auroral features. Quasi-periodic fluctuations with a periodicity close to 10 min (Ps6) and peak-to-peak variations up to 1,000 nT are seen during the passage of the features, especially in the E and E components. The spikes identified are associated with the E and E components are seen over many hours (Figures 6a and 6b), these particular magnetometer stations rotate out of the correct local time sector after 13 UT.

#### 3. Discussion

We have conducted a statistical study of the association of large dB/dt events with convection state during 2010, confirming that spikes occur preferentially in two distinct hot-spots in the pre-midnight (19–00 MLT) and dawn

MILAN ET AL. 12 of 16

sectors (03–07 MLT). Although 2010 was a geomagnetically quiet year, and the distribution of spikes is known to depend on phase of the solar cycle (e.g., Milan, Imber, et al., 2023), the 2010 distribution is consistent with several previous studies (e.g., Fleetham et al., 2024; Juusola et al., 2015; Kataoka & Pulkkinen, 2008; Milan, Imber, et al., 2023; Schillings et al., 2022; Viljanen et al., 2001; Weigel et al., 2002).

The pre-midnight hot-spot is expected to be associated with substorm onsets and the formation of the substorm current wedge, producing negative excursions in the north-south component of the magnetic field; examples are shown in Figure 2 of this paper and in Figure 6 of Milan, Imber, et al. (2023). Our statistics show that pre-midnight spikes are indeed associated with substorm onsets, either isolated onsets (our expansion phase state) or onsets that occur during ongoing activity (driven phase onsets occurring during driven phases). Such onsets can also occur during intervals classed as multiple intensifications. Substorms recur with timescales of several hours, and this modulates the occurrence of pre-midnight spikes. Pre-midnight spikes have also been observed during HILD-CAAs (Milan, Mooney, et al., 2023), which are periods of quasi-periodic substorms produced by high-speed solar wind streams (Tsurutani & Gonzalez, 1987).

Our statistics show that the dawn sector hot-spot is associated with geomagnetic activity classed as multiple intensifications in AL. These spikes have previously been attributed to Ps6 (10–20 min period) magnetic perturbations in the east-west component produced by omega bands (e.g., Apatenkov et al., 2020); examples are shown in Figures 2 and 7 of this study and Figure 7 of Milan, Imber, et al. (2023). Omega bands are azimuthally-spaced auroral intensifications which drift eastwards within the sunwards convection return flow, producing quasi-periodic magnetic fluctuations on the ground, mainly in the east-west component. Dawn spikes are most prevalent during strong solar wind driving, as will be discussed in more detail below. This dawnside activity can continue for many hours, producing quasi-continuous, quasi-periodic magnetic fluctuations on the ground. Strong driving is also conducive to causing substorms, so pre-midnight spikes can occur during ongoing dawn activity. However, there does not appear to be a direct link between the two phenomena. Schillings et al. (2022) surmised that during geomagnetic storms dawn sector spikes were preceded by pre-midnight spikes, that is omega band activity occurred subsequent to substorm activity. However, this does not appear to be the case in our observations.

Although dawn sector spikes have been attributed to omega bands, there is some discrepancy in the reported characteristics of the two phenomena. Omega band occurrence peaks at 02 to 03 MLT (e.g., Partamies et al., 2017; Vokhmyanin et al., 2021) whereas dawn spikes peak between 03 and 07 MLT. Indeed, Figure 3 and the study of Milan, Imber, et al. (2023) show a distinct dearth of spikes in the 01 to 02 MLT sector. Omega bands are thought to be associated with substorm onset (Wild et al., 2000) and substorm recovery phase (Vanhamäki et al., 2009), but we have shown that dawn spikes can occur independently of substorms. Typically, the omega band Ps6 magnetic signature has peak-to-peak values of a few 10 s nT (Sato et al., 2015) and average  $dB/dt \approx 50$  nT min<sup>-1</sup> (Vokhmyanin et al., 2021), though extreme examples have been reported with dB/dt of several 100 s nT min<sup>-1</sup> (Apatenkov et al., 2020). Most reported omega bands have a latitudinal extent of a few 100 s km (e.g., Vokhmyanin et al., 2021), consistent with the auroral emissions presented in Figure 6. However, we have also shown that spikes can be formed by features more resembling north-south aligned auroral streamers which can stretch over 15° of latitude, as presented in Figure 4. Indeed, a range of auroral activities occur in this local time sector and it is possible that omega bands and streamers are related (e.g., Henderson, 2022). Both phenomena occur in the same local time sector, both are azimuthally-spaced auroral intensifications, and both drift eastwards. A recent numerical simulation by Sorathia et al. (2023) has shown that streamers can be the auroral signature of bursty bulk flow (BBF) activity in the dawn sector associated with a "dawnside current wedge"; it was suggested in that study that these streamers could produce dawn sector spikes. Hence, it seems that the cause(s) of dawn sector spikes is broader than just omega bands, and that the relationship between omega bands and streamers should be investigated in more detail. Sorathia et al. (2023) suggested that such dawn activity could be caused by a dawn-dusk asymmetry in the ring current distribution, and this will be investigated in a subsequent study.

Omega bands propagate at speeds up to  $1,500\,\mathrm{m\,s^{-1}}$ , though  $500\,\mathrm{m\,s^{-1}}$  is more typical (Vokhmyanin et al., 2021). We expect that dawn sector auroral features (omega bands or streamers) are embedded within the convection return flow so drift at, or close to, the convection return flow speed. If they represent regions of high conductance within relatively laminar return flow then they will be associated with enhanced Hall currents, divergence of which at the edges of the features will lead to up/down pairs of FACs. This could explain the dawnside modulated FACs seen in Figure 1. Modulated Hall currents will also lead to ground magnetic perturbations. The dawnside

MILAN ET AL. 13 of 16

auroral features have an azimuthal spacing of approximately 1 hr of MLT (700 km) at both 01 and 12 UT in Figure 6. The periodicity of perturbations seen at a fixed MLT will then depend on the convection speed: a period of 10 min at a drift speed of 1 km s<sup>-1</sup> and 20 min at 500 m s<sup>-1</sup>, consistent with the Ps6 pulsations reported to be associated with omega bands (Rostoker et al., 1980) and with our observations (Figure 7). Higher convection speeds will lead to higher frequencies in the ground magnetic perturbations, which in turn will lead to higher dB/dt for quasi-periodic pulsations of fixed amplitude (see also Vokhmyanin et al. (2021); Milan, Imber, et al. (2023)). The features highlighted by arrows in Figure 6a at 01 and 12 UT propagate at different speeds and only the fast features at 12 UT produce spikes. Convection strength is driven by dayside reconnection:  $\Phi_D^{\star}$  is close to 200 kV at 12 UT when the features propagate rapidly and spikes are observed but only 100 kV at 01 UT when spikes are not observed and features propagate slowly. This could explain the preference of dawnside spikes for stronger solar wind driving, as seen in Figure 4 and reported by Milan, Imber, et al. (2023).

Dawn spikes were the most common type during 2010, 54%, although the multiple intensifications state occurred for less than 2% of the time. Expansion and driven phases, which accounted for the majority of the other 46% of spikes occupied 25% of the time. The rapid negative excursions seen in AL during multiple intensifications are not produced by the substorm electrojet in the pre-midnight sector but by features in the westward electrojet between 03 and 07 MLT. These are not substorm onsets, and are not necessarily directly associated with substorm onsets. However, they will be misidentified as substorm onsets by any substorm identification algorithm based solely on AL (e.g., Forsyth et al., 2015; Newell & Gjerloev, 2011), as shown in Figure 7 of Milan et al. (2019). Milan et al. (2021) coined the name "multiple intensifications" based on the misunderstanding that they represented reintensifications of on-going substorm activity. We should rename "multiple intensifications" as "westjet fluctuations" or something similar.

Our statistical survey hints at a third, minor, population of spikes near 07 MLT, which occur during high  $V_{SW}$  (Figure 4d). These spikes are presumably driven by the Kelvin-Helmholtz instability occurring on the dawn magnetopause flank (see Milan, Imber, et al., 2023; Weigel et al., 2003). The year 2010 was close to solar minimum and had low average  $V_{SW}$ , explaining the relative lack of such spikes in this study.

#### 4. Conclusions

The primary cause of GICs in conductors near the ground are occurrences of large and rapid changes in the ground magnetic field — large dB/dt events — produced by currents flowing in the ionosphere. Other factors are important in determining the magnitude of GICs, including ground conductivity, the orientation of the conductor, and the conductor network characteristics. These factors are not considered by our study. However, we have studied the occurrence of dB/dt spikes, which are necessary for the production of GICs, in SuperMAG observations. We conclude:

- In 2010, spikes occurred preferentially in two local time sectors, pre-midnight and dawn.
- Pre-midnight spikes appear predominantly in the N component. They occur simultaneously with substorm
  onsets observed in the AL index and identified in the convection state study of Milan et al. (2021).
- Dawn spikes are accompanied by strong, rapid variations in the AL index produced by activity in the dawn sector westward electrojet—these are not substorms, though are often misidentified as such.
- Dawn spikes and multiple intensifications in AL occurred during periods of strong solar wind driving with moderate solar wind speed but strongly-southward IMF.
- Pre-midnight and dawn spikes can occur independently, though they often occur together as the driving conditions necessary for dawn spikes also favor the excitation of substorms.
- Dawn spikes were associated with azimuthally-periodic auroral forms, sharing characteristics of omega bands and streamers, in the dawn sector which could extend over many degrees of latitude.
- These auroral forms propagate sunwards in the convection return flow; the speed of propagation presumably
  depends on the convection speed, which in turn will be related to the rate of dayside reconnection. The passage
  of these forms produces Ps6 magnetic pulsations on the ground, predominantly in the N and E components.
- Faster propagation will lead to larger dB/dt for fixed amplitude quasi-periodic magnetic perturbations, favoring spikes during strong convection.
- The auroral forms, their propagation, and the magnetic perturbations they produce are reminiscent of omega bands. However, they are larger than most reported omega bands, occur several hours of MLT eastwards of typical omega bands, and their magnetic perturbations are considerably larger.

MILAN ET AL. 14 of 16



Acknowledgments

SEM was supported by the Science and

Technology Facilities Council (STFC),

Natural Environment Research Council

(NERC), UK, Grant number NE/ W006766/1. ALF was supported by an

NASA/GSFC's Space Physics Data

Facility's CDAWeb service and OMNI data. For the purpose of open access, the author has applied a Creative Commons Attribution (CC BY) license to the Author

UK, Grant number ST/W00089X/1. SMI, GEB, and SEM were supported by the

STFC studentship. We acknowledge use of

Accepted Manuscript version arising from

this submission. For the SuperMAG ground magnetometer data we gratefully acknowledge: INTERMAGNET, Alan

Thomson; CARISMA, PI Ian Mann;

CANMOS, Geomagnetism Unit of the

Geological Survey of Canada; The S-

RAMP Database, PI K. Yumoto and Dr. K.

Shiokawa; The SPIDR database; AARI, PI Oleg Troshichev; The MACCS program,

PI M. Engebretson; GIMA; MEASURE,

Technology; SAMBA, PI Eftyhia Zesta;

210 Chain, PI K. Yumoto; SAMNET, PI Farideh Honary; IMAGE, PI Liisa Juusola;

Finnish Meteorological Institute, PI Liisa Juusola; Sodankylä Geophysical

Observatory, PI Tero Raita; UiT the Arctic

Geophysical Observatory, PI Magnar G. Johnsen: GFZ German Research Center

Institute of Geophysics, Polish Academy

of Sciences, PI Anne Neska and Jan Reda;

Polar Geophysical Institute, PI Alexander Yahnin and Yarolav Sakharov; Geological Survey of Sweden, PI Gerhard Schwarz;

Swedish Institute of Space Physics, PI

Masatoshi Yamauchi; AUTUMN, PI Martin Connors; DTU Space, Thom

Lanzarotti and Alan T. Weatherwax;

Edwards and PI Anna Willer; South Pole and McMurdo Magnetometer, PI's Louis J.

ICESTAR; RAPIDMAG; British Artarctic Survey; McMac, PI Dr. Peter Chi; BGS, PI

Dr. Susan Macmillan; Pushkov Institute of

Terrestrial Magnetism, Ionosphere and

Radio Wave Propagation (IZMIRAN); MFGI, PI B. Heilig; Institute of

Geophysics, Polish Academy of Sciences,

PI Anne Neska and Jan Reda; University of

Lesur and A. Chambodut; Data obtained in cooperation with Geoscience Australia, PI

Clauer and Michael Hartinger; MagStar, PI

W. Gjerloev; Data obtained in cooperation

Jennifer Gannon; SuperMAG, PI Jesper

with the Australian Bureau of Meteorology, PI Richard Marshall.

L'Aquila, PI M. Vellante; BCMT, V.

Andrew Lewis: AALPIP, co-PIs Bob

For Geosciences, PI Jürgen Matzka;

University of Norway, Tromsø

UCLA IGPP and Florida Institute of

### **Journal of Geophysical Research: Space Physics**

10.1029/2024JA032811

A simulation by Sorathia et al. (2023) suggests that such auroral features are associated with the formation of a
dawn sector current wedge and bursty bulk flow activity. However, the similarity to omega bands suggests
some unified mechanism should be able to explain both phenomena (e.g., Henderson, 2022). The possible
relation of these features to a dawn-dusk asymmetry in the ring current distribution should be investigated.

#### **Data Availability Statement**

The high resolution (1-min) OMNI data used in this study were obtained from the NASA Goddard Space Flight Center (GSFC) Space Physics Data Facility OMNIWeb portal at https://omniweb.gsfc.nasa.gov/form/om\_filt\_min.html). The 1-min cadence ("low fidelity") SuperMAG data were obtained from NASA GSFC through the SuperMAG portal at https://supermag.jhuapl.edu/mag/?fidelity=low. The IMAGE WIC data were obtained from CDAWeb (https://cdaweb.gsfc.nasa.gov). The DMSP/SSUSI file type EDR-AUR data were obtained from http://ssusi.jhuapl.edu (data version 0106, software version 7.0.0, calibration period version E0018). AMPERE data were obtained from http://ampere.jhuapl.edu. The DMSP/SSIES data were downloaded from the Madrigal Database at Millstone Hill (http://millstonehill.haystack.mit.edu).

#### References

Akasofu, S.-I. (1964). The development of the auroral substorm. Planetary and Space Science, 12(4), 273–282. https://doi.org/10.1016/0032-0633

Anderson, B., Takahashi, K., & Toth, B. (2000). Sensing global Birkeland currents with Iridium® engineering magnetometer data. *Geophysical Research Letters*, 27(24), 4045–4048. https://doi.org/10.1029/2000GL000094

Apatenkov, S., Pilipenko, V., Gordeev, E., Viljanen, A., Juusola, L., Belakhovsky, V., et al. (2020). Auroral omega bands are a significant cause of large geomagnetically induced currents. *Geophysical Research Letters*, 47(6), e2019GL086677. https://doi.org/10.1029/2019GL086677

Chisham, G., Freeman, M., Abel, G., Lam, M., Pinnock, M., Coleman, I., et al. (2008). Remote sensing of the spatial and temporal structure of magnetopause and magnetotail reconnection from the ionosphere. *Reviews of Geophysics*, 46(1). https://doi.org/10.1029/2007RG000223

Cowley, S., & Lockwood, M. (1992). Excitation and decay of solar wind-driven flows in the magnetosphere-ionosphere system. Annales Geophysicae, 10, 103–115.

Davis, T. N., & Sugiura, M. (1966). Auroral electrojet activity index AE and its universal time variations. *Journal of Geophysical Research*, 71(3), 785–801. https://doi.org/10.1029/jz071i003p00785

Dungey, J. (1961). Interplanetary magnetic field and the auroral zones. *Physical Review Letters*, 6(2), 47–48. https://doi.org/10.1103/ PhysRevLett.6.47

Engebretson, M., Kirkevold, K., Steinmetz, E., Pilipenko, V. A., Moldwin, M., McCuen, B., et al. (2020). Interhemispheric comparisons of large nighttime magnetic perturbation events relevant to GICs. *Journal of Geophysical Research: Space Physics*, 125(8), e2020JA028128. https://doi.org/10.1029/2020JA028128

Fleetham, A., Milan, S., Imber, S., Bower, G., Gjerloev, J., & Vines, S. (2024). The relationship between large dB/dt and field-aligned currents during five geomagnetic storms. *Journal of Geophysical Research: Space Physics*, 129(7), e2024JA032483. https://doi.org/10.1029/2004JA032483

Forsyth, C., Rae, I., Coxon, J., Freeman, M., Jackman, C., Gjerloev, J., & Fazakerley, A. (2015). A new technique for determining substorm onsets and phases from indices of the electrojet (SOPHIE). *Journal of Geophysical Research: Space Physics*, 120(12), 10–592. https://doi.org/10.1002/2015ja021343

Gjerloev, J. (2012). The SuperMAG data processing technique. *Journal of Geophysical Research*, 117(A9). https://doi.org/10.1029/2012JA017683

Gonzalez, W., Joselyn, J.-A., Kamide, Y., Kroehl, H., Rostoker, G., Tsurutani, B., & Vasyliunas, V. (1994). What is a geomagnetic storm? *Journal of Geophysical Research*, 99(A4), 5771–5792. https://doi.org/10.1029/93JA02867

Henderson, M. G. (2022). Association of mesoscale auroral structures and breakups with energetic particle injections at geosynchronous orbit. Frontiers in Astronomy and Space Sciences, 9, 742246. https://doi.org/10.3389/fspas.2022.742246

Hubert, B., Milan, S., Grocott, A., Blockx, C., Cowley, S., & Gérard, J.-C. (2006). Dayside and nightside reconnection rates inferred from IMAGE FUV and super dual auroral radar network data. *Journal of Geophysical Research*, 111(A3). https://doi.org/10.1029/2005JA011140

Iijima, T., & Potemra, T. (1976). The amplitude distribution of field-aligned currents at northern high latitudes observed by Triad. Journal of Geophysical Research, 81(13), 2165–2174. https://doi.org/10.1029/JA081i013p02165

Iyemori, T. (1990). Storm-time magnetospheric currents inferred from mid-latitude geomagnetic field variations. *Journal of Geomagnetism and Geoglectricity*, 47(11), 1249–1265. https://doi.org/10.5636/j.gg.42.1249

Geoelectricity, 42(11), 1249–1265. https://doi.org/10.5636/jgg.42.1249

Juusola, L., Viljanen, A., Van De Kamp, M., Tanskanen, E., Vanhamäki, H., Partamies, N., & Kauristie, K. (2015). High-latitude ionospheric equivalent currents during strong space storms: Regional perspective. Space Weather, 13(1), 49–60. https://doi.org/10.1002/2014SW001139

Kataoka, R., & Pulkkinen, A. (2008). Geomagnetically induced currents during interacting regions. *Journal of Geophysical Research*, 113(A3). https://doi.org/10.1029/2007JA012487

Mende, S., Heetderks, H., Frey, H., Lampton, M., Geller, S., Abiad, R., et al. (2000). Far ultraviolet imaging from the IMAGE spacecraft. 2. Wideband FUV imaging. *Space Science Reviews*, 91(1/2), 271–285. https://doi.org/10.1023/A:1005227915363

Milan, S. (2019). AMPERE R1/R2 FAC radii Dataset. Figshare. https://doi.org/10.25392/leicester.data.11294861.v1

Milan, S. (2020). Magnetospheric geonome project 2010 University of Leicester Dataset. https://doi.org/10.25392/leicester.data.12571307.v1
Milan, S., Carter, J., Korth, H., & Anderson, B. (2015). Principal component analysis of Birkeland currents determined by the active magnetosphere and planetary Electrodynamics Response experiment. *Journal of Geophysical Research: Space Physics*, 120(12), 10–415. https://doi.org/10.1002/2015JA021680

Milan, S., Carter, J., Sangha, H., Bower, G., & Anderson, B. (2021). Magnetospheric flux throughput in the Dungey cycle: Identification of convection state during 2010. *Journal of Geophysical Research: Space Physics*, 126(2), e2020JA028437. https://doi.org/10.1029/2020JA028437

MILAN ET AL. 15 of 16

- Milan, S., Clausen, L., Coxon, J., Carter, J., Walach, M.-T., Laundal, K., et al. (2017). Overview of solar wind–magnetosphere–ionosphere–atmosphere coupling and the generation of magnetospheric currents. *Space Science Reviews*, 206(1–4), 547–573. https://doi.org/10.1007/s11214-017-0333-0
- Milan, S., Gosling, J., & Hubert, B. (2012). Relationship between interplanetary parameters and the magnetopause reconnection rate quantified from observations of the expanding polar cap. *Journal of Geophysical Research*, 117(A3), https://doi.org/10.1029/2011JA017082
- Milan, S., Imber, S., Fleetham, A., & Gjerloev, J. (2023a). Solar cycle and solar wind dependence of the occurrence of large dB/dt events at high latitudes. *Journal of Geophysical Research: Space Physics*, 128(4), e2022JA030953. https://doi.org/10.1029/2022JA030953
- Milan, S., Mooney, M., Bower, G., Fleetham, A., Vines, S., & Gjerloev, J. (2023b). Solar wind-magnetosphere coupling during high-intensity long-duration continuous AE activity (HILDCAA). *Journal of Geophysical Research: Space Physics, 128*(11), e2023JA032027. https://doi.org/10.1029/2023JA032027
- Milan, S., Provan, G., & Hubert, B. (2007). Magnetic flux transport in the Dungey cycle: A survey of dayside and nightside reconnection rates. Journal of Geophysical Research, 112(A1). https://doi.org/10.1029/2006JA011642
- Milan, S., Walach, M.-T., Carter, J., Sangha, H., & Anderson, B. (2019). Substorm onset latitude and the steadiness of magnetospheric convection. Journal of Geophysical Research: Space Physics, 124(3), 1738–1752. https://doi.org/10.1029/2018JA025969
- Molinski, T., Feero, W., & Damsky, B. (2000). Shielding grids from solar storms. *IEEE Spectrum*, 37(11), 55–60. https://doi.org/10.1109/6.880955
- Newell, P., & Gjerloev, J. (2011). Evaluation of SuperMAG auroral electrojet indices as indicators of substorms and auroral power. *Journal of Geophysical Research*, 116(A12). https://doi.org/10.1029/2011ja016779
- Ngwira, C. M., Sibeck, D., Silveira, M. V., Georgiou, M., Weygand, J. M., Nishimura, Y., & Hampton, D. (2018). A study of intense local dB/dt variations during two geomagnetic storms. *Space Weather*, 16(6), 676–693. https://doi.org/10.1029/2018SW001911
- Papitashvili, N., & King, J. (2020). Omni 1-min dat [Dataset]. NASA Space Physics Data Facility. https://doi.org/10.48322/45bb-8792
- Partamies, N., Weygand, J., & Juusola, L. (2017). Statistical study of auroral omega bands. Annales Geophysicae, 35(5), 1069–1083. https://doi.org/10.5194/angeo-35-1069-2017
- Paxton, L., Meng, C.-I., Fountain, G., Ogorzalek, B., Darlington, E., Gary, S., et al. (1992). Special sensor ultraviolet spectrographic imager: An instrument description. In *Instrumentation for Planetary and Terrestrial Atmospheric Remote Sensing* (Vol. 1745, pp. 2–15). https://doi.org/10.1117/12.60595
- Pulkkinen, A., & Kataoka, R. (2006). S-transform view of geomagnetically induced currents during geomagnetic superstorms. Geophysical Research Letters, 33(12). https://doi.org/10.1029/2006GL025822
- Rajaram, G., Rostoker, G., & Samson, J. (1986). Wave characteristics of Ps 6 magnetic variations and their implications for convective flow in the magnetotail. *Planetary and Space Science*, 34(3), 319–329. https://doi.org/10.1016/0032-0633(86)90138-8
- Rich, F., & Hairston, M. (1994). Large-scale convection patterns observed by DMSP. *Journal of Geophysical Research*, 99(A3), 3827–3844. https://doi.org/10.1029/93JA03296
- Rostoker, G., Akasofu, S.-I., Foster, J., Greenwald, R., Kamide, Y., Kawasaki, K., et al. (1980). Magnetospheric substorms—Definition and signatures. *Journal of Geophysical Research*, 85(A4), 1663–1668. https://doi.org/10.1029/JA085iA04p01663
- Rostoker, G., & Barichello, J. (1980). Seasonal and diurnal variation of Ps 6 magnetic disturbances. *Journal of Geophysical Research*, 85(A1), 161–163, https://doi.org/10.1029/JA085iA01p00161
- Sato, N., Kadokura, A., Tanaka, Y., Nishiyama, T., Hori, T., & Yukimatu, A. S. (2015). Omega band pulsating auroras observed onboard themis spacecraft and on the ground. *Journal of Geophysical Research: Space Physics*, 120(7), 5524–5544. https://doi.org/10.1002/2015JA021382
- Schillings, A., Palin, L., Opgenoorth, H., Hamrin, M., Rosenqvist, L., Gjerloev, J., et al. (2022). Distribution and occurrence frequency of dB/dt spikes during magnetic storms 1980-2020. Space Weather, 20(5), e2021SW002953. https://doi.org/10.1029/2021SW002953
- Sergeev, V., Pellinen, R. J., & Pulkkinen, T. (1996). Steady magnetospheric convection: A review of recent results. Space Science Reviews, 75(3–4), 551–604. https://doi.org/10.1007/BF00833344
- Sorathia, K., Michael, A., Merkin, V., Ohtani, S., Keesee, A., Sciola, A., et al. (2023). Multiscale magnetosphere-ionosphere coupling during stormtime: A case study of the dawnside current wedge. *Journal of Geophysical Research: Space Physics*, 128(11), e2023JA031594. https://doi.org/10.1029/2023JA031594
- Troshichev, O., Janzhura, A., & Stauning, P. (2006). Unified PCN and PCS indices: Method of calculation, physical sense, and dependence on the IMF azimuthal and northward components. *Journal of Geophysical Research*, 111(A5). https://doi.org/10.1029/2005JA011402
- Tsurutani, B., & Gonzalez, W. (1987). The cause of high-intensity long-duration continuous AE activity (HILDCAAs): Interplanetary Alfvén wave trains. *Planetary and Space Science*, 35(4), 405–412. https://doi.org/10.1016/0032-0633(87)90097-3
- Vanhamäki, H., Kauristie, K., Amm, O., Senior, A., Lummerzheim, D., & Milan, S. (2009). Electrodynamics of an omega-band as deduced from optical and magnetometer data. *Annales Geophysicae*, 27(9), 3367–3385. https://doi.org/10.5194/angeo-27-3367-2009
- Viljanen, A., Nevanlinna, H., Pajunpää, K., & Pulkkinen, A. (2001). Time derivative of the horizontal geomagnetic field as an activity indicator. Annales Geophysicae, 19(9), 1107–1118. https://doi.org/10.5194/angeo-19-1107-2001
- Vokhmyanin, M., Apatenkov, S., Gordeev, E., Andreeva, V., Partamies, N., Kauristie, K., & Juusola, L. (2021). Statistics on omega band properties and related geomagnetic variations. *Journal of Geophysical Research: Space Physics*, 126(7), e2021JA029468. https://doi.org/10.1029/2021JA029468
- Waters, C., Anderson, B., & Liou, K. (2001). Estimation of global field aligned currents using the Iridium® system magnetometer data. Geophysical Research Letters, 28(11), 2165–2168. https://doi.org/10.1029/2000GL012725
- Weigel, R., Klimas, A., & Vassiliadis, D. (2003). Solar wind coupling to and predictability of ground magnetic fields and their time derivatives. *Journal of Geophysical Research*, 108(A7). https://doi.org/10.1029/2002JA009627
- Weigel, R., Vassiliadis, D., & Klimas, A. (2002). Coupling of the solar wind to temporal fluctuations in ground magnetic fields. Geophysical Research Letters, 29(19), 21. https://doi.org/10.1029/2002GL014740
- Wild, J., Yeoman, T., Eglitis, P., & Opgenoorth, H. (2000). Multi-instrument observations of the electric and magnetic field structure of omega bands. *Annales Geophysicae*, 18(1), 99–110. https://doi.org/10.1007/s00585-000-0099-6
- Zou, Y., Dowell, C., Ferdousi, B., Lyons, L., & Liu, J. (2022). Auroral drivers of large dB/dt during geomagnetic storms. Space Weather, 20(11), e2022SW003121. https://doi.org/10.1029/2022SW003121

MILAN ET AL. 16 of 16